# Manganese- and Cobalt-Based Coordination Networks as Promising Heterogeneous Catalysts for Olefin Epoxidation Reactions

Girijesh Kumar,[†] Gulshan Kumar,[†] and Rajeev Gupta*

Department of Chemistry, University of Delhi, Delhi 110 007, India

S *Supporting Information*

ABSTRACT: We demonstrate the synthesis of Mn^{2+}- and Co^{2+}-based coordination networks using two Co^{3+}-based metalloligands differing by the position of the appended arylcarboxylate groups. The structural analyses reveal topologically distinct networks with pores of variable dimensions allowing facile diffusion of substrates and/or reagents. All four networks function as heterogeneous catalysts for the olefin epoxidation reactions using *tert*-butyl-hydroperoxide without any requirement of solvent or additive. Control and optimization experiments illustrate recyclable network-based catalysts that make them attractive candidates for the "greener" oxidation chemistry processes.
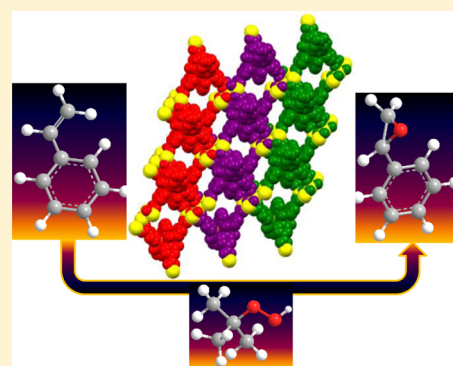
INTRODUCTION

In recent time, research on crystalline porous materials has received significant attention due to their well-defined architecture[1] and potential applications in gas sorption and storage,[2] separation,[3] sensing,[4] ion exchange,[5] molecular transport and delivery,[6] optics,[7] molecular magnetism,[8] devices,[9] and catalysis.[10] In particular, their utilization as heterogeneous catalysts in assorted organic transformation reactions has shown noteworthy results due to the optimized control of void space available within such crystalline porous materials.[11] Importantly, such catalytic properties are largely possible due to the crystalline nature of networks and therefore orderly arrangement of catalytic sites and the presence of well-defined pores and channels for a better substrate and/or reagent accessibility.[10,11d] For catalysis, it is imperative that the catalytic sites are either coordinatively unsaturated or ligated by easily dissociable solvent molecules while it is further advantageous to design a material to circumvent the catenation which prevents accessibility of the substrates and/or reagents to the catalytic sites. Unification of such critical features is often challenging to incorporate in a material via traditional solvothermal synthesis involving organic ligands and metal ions; however, a well-designed metalloligand[12] promises to include several of the mentioned parameters to afford a desirable catalytic material.

Metal-catalyzed oxidation reactions are one of the most important reactions in chemistry.[13] In particular, olefin epoxidation[14] has received considerable interest from both research and industry as epoxides play an eminent role as intermediates and buildings blocks in organic synthesis.[15] In this context, manganese and cobalt complexes have been particularly studied as the oxidation catalysts for the epoxidation reactions.[16] Some of the well-studied metal complexes are those based on porphyrin[17] and salen systems,[18] although both manganese and cobalt complexes with nonheme ligands have also been utilized in oxidation reactions.[19] An important challenge is to heterogenize a homogeneous catalyst as the conventional homogeneous catalysis is undesirable both from an industrial-scale and from an environmental viewpoint due to the excessive use of solvents and reagents.[20] In addition, aerobic[21] and peroxidative[22] oxidations of olefins are regarded as the simplest yet efficient epoxidation methods rather than the use of hazardous and inefficient oxo-transfer reagents.[21,22]

Our research group has developed assorted coordination complexes as the metalloligands,[12] offering secondary functional groups and/or coordination sites, for the construction of ordered architectures.[23−25] These metalloligands on reaction with secondary metal ions afford two- (2D) and three-dimensional (3D) networks[25] as well as layered materials.[25f] Our metalloligand approach provides precise control over the placement of Lewis-acidic secondary metal sites in the resultant networks in an exclusively noncatenated manner.[24,25] Such an approach has helped us in showcasing Lewis-acid-catalyzed reactions in substrate-specific[24] and regio-,[24,25a−c,e−g] stereo-,[25e−g] and size-selective[25e,f] manner. Inspired by the successful Lewis-acidic catalytic results, we were naturally inclined to incorporate oxidation-sensitive secondary metals in the coordination networks. Herein we report the syntheses and characterization of {$Co^{3+}−Mn^{2+}$} and {$Co^{3+}−Co^{2+}$} coordination networks and their applications in the solvent-free heterogeneous epoxidation reactions.

Scheme 1. Synthetic Routes for Networks 3−6
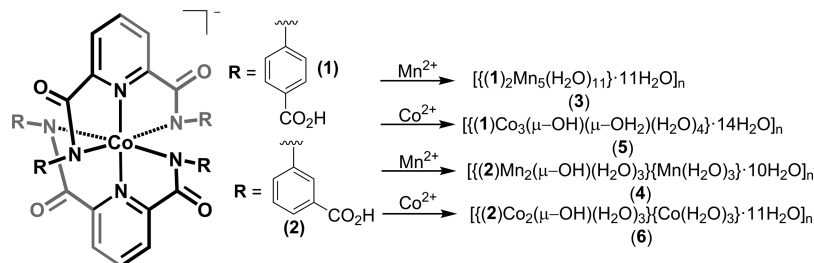
■ EXPERIMENTAL DETAILS

Materials and Methods. All commercially available reagents were of analytical grade and used as received without further purification. Solvents were purified using the standard literature procedure.[26] The lignads, $H_2L^{p\text{-COOH}}$ (2,6-bis(4-benzoicacid-carbomyl)pyridine)) and $H_2L^{m\text{-COOH}}$ (2,6-bis(3-benzoicacid-carbomyl)pyridine)), and their metalloligands, $Et_4N[Co(L^{p\text{-COOH}})_2]$ **1** and $Et_4N[Co(L^{m\text{-COOH}})_2]$ **2**, were synthesized as per our earlier reports.[2,5e,f]

Synthesis of $[\{(1)_2Mn_5(H_2O)_{11}\}\cdot 11H_2O]_n$ (3). Network **3** was synthesized by the reaction between $Mn(OAc)_2\cdot 4H_2O$ (61.52 mg, 0.2510 mmol) and metalloligand **1** (100 mg, 0.1004 mmol) in CH_3OH (10 mL). This reaction afforded a brown-colored product which was dissolved in water, filtered, and layered with tert-butyl alcohol at room temperature. After 4−5 days, deep green-colored crystals of **3**, suitable for diffraction studies, were collected by filtration. Yield (based on **1**): 0.224 g (81%). Anal. Calcd for $C_{84}H_{66}Co_2Mn_5N_{12}O_{57}\cdot 11H_2O$: C, 36.74; H, 3.23; N, 6.12. Found: C, 36.16; H, 3.12; N, 6.05. FTIR spectrum (Zn−Se ATR, selected peaks): 3412 (OH), 1602 (COO), 1569 (C=O) cm^{-1}. Absorption spectrum (solid state, λ_{max}/nm): 605, 578, 542.

Synthesis of $[\{(2)Mn_2(\mu\text{-OH})(H_2O)_3\}\{Mn(H_2O)_3\}\cdot 10H_2O]_n$ (4). Network **4** was prepared in a similar manner with a similar scale as that of network **3**, however, using metalloligand **2** in place of **1**. Reddish-green-colored crystals of **4** were collected after a period of 5−6 days. Yield (based on **2**): 0.218 g (84%). Anal. Calcd for $C_{42}H_{57}CoMn_3N_6O_{30}\cdot 10H_2O$: C, 32.97; H, 5.07; N, 5.49. Found: C, 32.56; H, 5.17; N, 5.57. FTIR spectrum (Zn−Se ATR, selected peaks): 3212 (OH), 1555 (COO, C=O) cm^{-1}. Absorption spectra (solid state, λ_{max}/nm): 604, 579, 538.

Synthesis of $[\{(1)Co_3(\mu\text{-OH})(\mu\text{-}H_2O)(H_2O)_4\}\cdot 14H_2O]_n$ (5). Network **5** was also synthesized in a similar manner with a similar scale as that of network **3**, however using $Co(OAc)_2\cdot 2H_2O$ in place of $Mn(OAc)_2\cdot 4H_2O$. Deep green-colored crystals of network **5** were obtained after a period of 5−6 days. Yield (based on **1**): 0.225 g (83%). Anal. Calcd for $C_{42}H_{41}Co_4N_6O_{22}\cdot 14H_2O$: C, 34.32; H, 4.73; N, 5.72. Found: C, 34.37; H, 4.61; N, 5.28. FTIR spectrum (Zn−Se ATR, selected peaks): 3335 (OH), 1602 (COO), 1563 (C=O) cm^{-1}. Absorption spectrum (solid state, λ_{max}/nm): 620, 584, 547.

Synthesis of $[\{(2)Co_2(\mu\text{-OH})(H_2O)_3\}\{Co(H_2O)_3\}\cdot 11H_2O]_n$ (6). Network **6** was prepared in a similar fashion with a similar scale as that of network **5**, however using metalloligand **2**. Deep brown-colored crystals of network **6** were obtained after a period of 3−4 days. Yield (based on **2**): 0.238 g (90%). Anal. Calcd for $C_{42}H_{35}Co_4N_6O_{19}\cdot 11H_2O$: C, 37.05; H, 4.22; N, 6.17. Found: C, 37.15; H, 4.45; N, 6.22. FTIR spectrum (Zn−Se ATR, selected peaks): 3350 (OH), 1560 (COO, C=O) cm^{-1}. Absorption spectrum (solid state, λ_{max}/nm): 609, 566, 538.

General Procedure for the Exchange Studies. A batch of 100 mg of powdered sample was taken in a glass vial and heated at 150 °C (using oil bath) under vacuum for 8 h. Subsequently, the glass vial containing sample was sealed in a bigger glass vial containing 2 mL of D_2O (or any other substrate). The sealed sample was allowed to equilibrate with D_2O vapors (or any other substrate) for 24 h. Finally, the sample was dried under vacuum and characterized.

General Procedure for the Inclusion Studies. Batches of sample ranging from 20 to 50 mg were impregnated by suspending them in a CH_2Cl_2 solution containing 10 equiv of a substrate for 12 h at 25 °C. The impregnated sample was washed thrice with fresh CH_2Cl_2, dried under vacuum, and characterized.

General Procedure for the Olefin Epoxidation Reaction. In a typical olefin epoxidation reaction, 100 μL of the corresponding olefin was treated with tert-butyl hydroperoxide (TBHP) in a 1:3 ratio in the presence of 2 mol % of catalyst (network **3**, **4**, **5**, or **6**) at 50 °C under the solvent-free conditions. The progress of the reaction was monitored by thin-layer chromatography (TLC) and/or gas chromatograph (GC). The reaction was quenched by adding 2 mL of EtOAc that led to the precipitation of solid catalyst which was filtered off and dried. The recovered catalysts were characterized by FTIR spectra and X-ray powder diffraction (XRPD) patterns that showed identical results to that of freshly prepared samples. The EtOAc layer was washed with water and dried over anhydrous Na_2SO_4, and the organic products were isolated after removal of solvent. The crude organic products were purified by the flash column chromatography on silica gel using 5% EtOAc/hexanes as the eluent. The products were analyzed and quantified by the GC/GC-MS techniques as well as proton NMR spectra in a few representative cases. For control experiments, reactions were performed to evaluate the role of (a) oxidizing agent, (b) solvent, (c) additive, (d) aerobic versus anaerobic environment, (e) catalyst loading, (f) reaction time, and (g) reaction temperature.

Physical Methods. The FTIR spectra were recorded with a PerkinElmer Spectrum-Two spectrometer (Zn−Se ATR; 4000−600 cm^{-1}). The diffuse reflectance spectra were recorded with a Lambda-35 spectrophotometer. The elemental analysis data were obtained with an Elementar Analysen Systeme GmbH Vario EL-III instrument. GC and GC-MS studies were performed using a PerkinElmer Clarus 580 with an Elite-5 column and Shimadzu instrument (QP 2010) with an RTX-5SIL-MS column, respectively. Thermal gravimetric analysis (TGA) and differential scanning calorimetry (DSC) were performed with DTG-60 Shimadzu and TA-DSC Q200 instruments, respectively, at a 5 °C min^{-1} heating rate under a nitrogen atmosphere. The XRPD studies were performed either on a Bruker AXS D8 Discover instrument or an X'Pert Pro from Panalytical (Cu Kα radiation, λ = 1.54184 Å). The samples were ground and subjected to the range of θ = 5−50° with a scan rate of 1°/min at room temperature.

Crystallography. The single-crystal X-ray diffraction data for networks 3−6 were collected on an Oxford XCalibur CCD diffractometer using graphite-monochromated Mo Kα radiation (λ = 0.71073 Å).[27] The frames were collected at 298(2) K for all four networks. Data was processed with XCalibur, while the empirical absorption correction was applied using spherical harmonics implemented in the SCALE3 ABSPACK scaling algorithm.[27] The structures were solved by direct methods using SIR-97[28] and refined by full-matrix least-squares refinement techniques on F^2 using the program SHELXL-97[29] incorporated in the WINGX 1.8.05 crystallographic collective package.[30] The non-hydrogen atoms were refined anisotropically, whereas the hydrogen atoms were fixed at the calculated positions with isotropic thermal parameters. For all four networks, hydrogen atoms of the bridging hydroxide, bridging water, and coordinated and uncoordinated water molecules could not be located from the difference Fourier map. Although hydrogen atoms of these moieties were not located, their numbers have been included in the empirical formulas of every network. The solvent-accessible voids
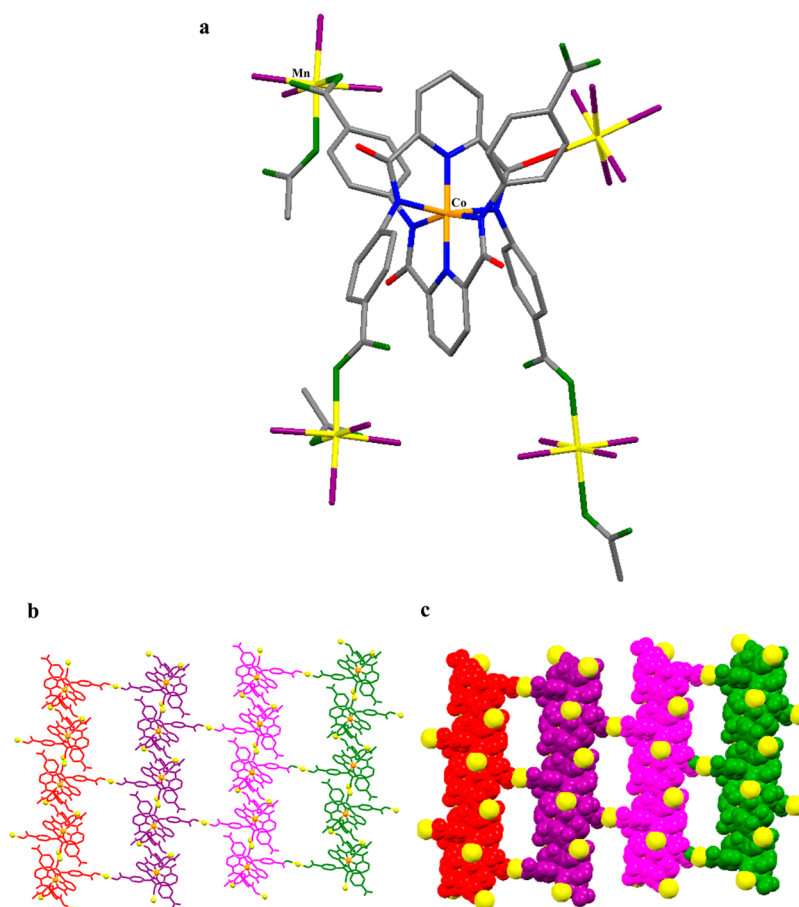
Figure 1. (a) Stick representation of a selected part of the crystal structure of network **3**. Color code: orange, Co; yellow, Mn; blue, N; green, $O_{carboxylate}$; purple, O_{water}; red, O_{amide}; gray, C. (b) Packing diagram in a view along the *a* axis. (c) Space-filling view along the *a* axis showing pores and channels in the structure of network **3**; the coordinated water molecules are omitted for clarity to show Mn^{2+} ions (yellow spheres).

(SAVs) were calculated using PLATON.[31] The details of the single-crystal X-ray diffraction data collection and structure solution parameters for networks **3–6** are provided in Table S1 (Supporting Information).

RESULTS AND DISCUSSION

Synthesis and Cherecterization. The heterobimetallic networks **3–6** have been synthesized by treating metalloligands $Et_4N[Co(L^{p\text{-}COOH})_2]$ (**1**) and $Et_4N[Co(L^{m\text{-}COOH})_2]$ (**2**) with the $M(OAc)_2$ salt (Scheme 1). In each case, reaction with the secondary metal salt resulted in a distinct color change followed by precipitation of the product. All four networks exhibited strong bands between 1561 and 1602 cm^{-1} due to the ν_{COO} stretches in their FTIR spectra.[25e,f,32] In addition, broad features between 3212 and 3412 cm^{-1} are indicative of the presence of coordinated as well as lattice water molecules.[25e,f,32] Networks **3–6** displayed λ_{max} in the range of 620–650 nm in their diffuse-reflectance spectra which are tentatively assigned to the d–d transitions (Figures S1 and S2, Supporting Information). The XRPD patterns of the freshly prepared samples of networks **3–6** are nearly identical to those simulated from the single-crystal structures indicative of the phase purity of the bulk samples (Figures S3–S6, Supporting Information). However, certain differences observed in diffraction line intensities can be attributed to the variation of the preferred orientation of crystallites in the powdered samples.

Crystal Structures. All four heterobimetallic networks were characterized by the single-crystal diffraction studies to understand the network generation via the mediation of metalloligands offering arylcarboxylate fragments. The metalloligand part in the crystal structures of all four networks is nearly identical and shows that the central Co^{3+} ion is meridionally coordinated by two tridentate ligands.[23−25] The central Co^{3+} ion is bonded to four N_{amide} atoms in the basal plane and two $N_{pyridine}$ atoms in the axial position with a compressed octahedral geometry.[23−25] The Co−N_{amide} bond distances are longer than the Co−$N_{pyridine}$ distances.[23−25] Two axial pyridine rings are trans to each other, whereas diagonal N_{amide} groups make an angle with the Co^{3+} ion larger than 160° in all cases. The crystal structures of {Co^{3+}−Mn^{2+}} and {Co^{3+}−Co^{2+}} networks from the metalloligands offering either *p*- or *m*-arylcarboxylate groups have notable similarity and are therefore discussed in that manner. Importantly, in all four networks, the appended groups are present in their completely deprotonated arylcarboxylate form and are involved in coordinating the secondary metal ions. In the case of networks **3** and **5** (with *p*-arylcarboxylate groups), however, one of the arylcarboxylate groups remains uncoordinated. For all four networks, Figures 1−4 provide drawings of the crystal structures, whereas Figures S7−S10, Supporting Information, display additional drawings with complete numbering scheme. Further, Table 1 displays the range noted for the bond distances, whereas Tables S2−S5, Supporting Information, provide the detailed bonding parameters for all four networks.

Crystal Structures of {Co^{3+}−Mn^{2+}} (3) and {Co^{3+}−Co^{2+}} (5) Networks with Metalloligands Offering *p*-Arylcar-
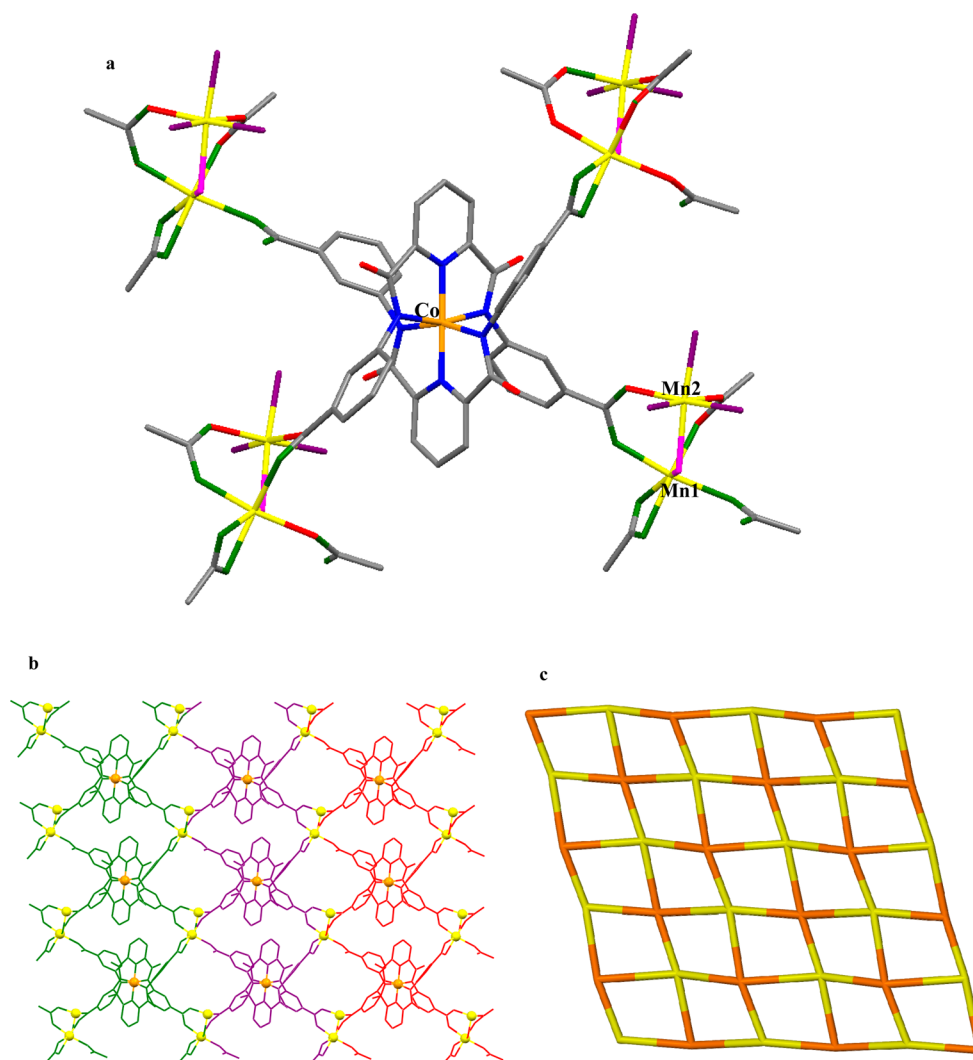
Figure 2. (a) Stick representation of a selected part of the crystal structure of network **4**. Color code: orange, Co; yellow, Mn; blue, N; green, $O_{carboxylate}$; purple, OH; red, O_{amide}; gray, C. (b) Packing diagram in a view along the b axis; coordinated water molecules are omitted for clarity to show Mn^{2+} ions (yellow spheres). (c) Topological representation of the network. Color code: orange, central Co^{3+} core as the node; yellow, Mn_2 cluster as the node.

boxylate Groups. Both networks **3** and **5** crystallized in a triclinic cell with $P\bar{1}$ space group. The asymmetric unit of network **3** contains 1 metalloligand, 3 Mn^{2+} ions, and 11 coordinated and 11 lattice water molecules, while **5** displays the presence of 1 metalloligand, 3 Co^{2+} ions, 1 bridging hydroxo, 1 bridging aqua, and 4 coordinated and 14 uncoordinated water molecules. The structures of networks **3** and **5** illustrate that the metalloligands are connected through the secondary metal ions resulting in 3D architectures. For **3**, every metalloligand offers four p-arylcarboxylate groups, and three of them assist in the coordination of three different Mn^{2+} ions, while the fourth one remains free. Every Mn^{2+} ion shows six-coordinated distorted octahedral geometry ligated by a certain number of $O_{carboxylate}$ atoms in addition to a few water molecules. Interestingly, coordination of metalloligands to that of Mn1 and Mn3 atoms results in the creation of one-dimensional chains, whereas Mn2 ions connect such chains to generate a network with large pores with cross sections of 19.96×18.50 Å^2. In the case of **5**, arylcarboxylate fragments from a metalloligand hold a {Co$_5$} cluster in which individual Co^{2+} ions are bridged by a μ_3-OH and a μ_2-OH$_2$ synthon in addition to a typical μ-1,2-carboxylate

bridge. The μ_3-OH group acts as a bridge between Co1, Co2, and Co3 ions, whereas a μ_2-OH$_2$ moiety additionally bridges Co2 and Co3 ions. For all three cobalt atoms, the remaining coordination sites are satisfied by $O_{carboxylate}$, while both Co1 and Co2 ions are also coordinated by two terminal water molecules. Network **5** displays two types of pores with dimensions of 11.15×7.46 and 11.83×11.69 Å^2, respectively.

Crystal Structures of {Co^{3+}–Mn^{2+}} (4) and {Co^{3+}–Co^{2+}} (6) Networks with Metalloligands Offering *m*-Arylcarboxylate Groups. The networks **4** and **6** crystallized in a monoclinic cell with $P2_1/n$ space group. Interestingly, both networks show an identical unit cell as well as molecular structure. The unit cells show the presence of 1 metalloligand, 3 secondary metal ions (Mn^{2+} or Co^{2+}), 1 bridging hydroxo, and 6 coordinated and 10 (for **4**) or 11 (for **6**) lattice water molecules. In both **4** and **6**, all four arylcarboxylate groups assist in coordinating a pair of secondary M^{2+} ions that result in a 2D architecture running in the crystallographic b axis. Both six-coordinated secondary M^{2+} ions display a typical paddle-wheel structure additionally bridged by a μ-OH group, however, differing by the arrangement of terminal ligands. One of the
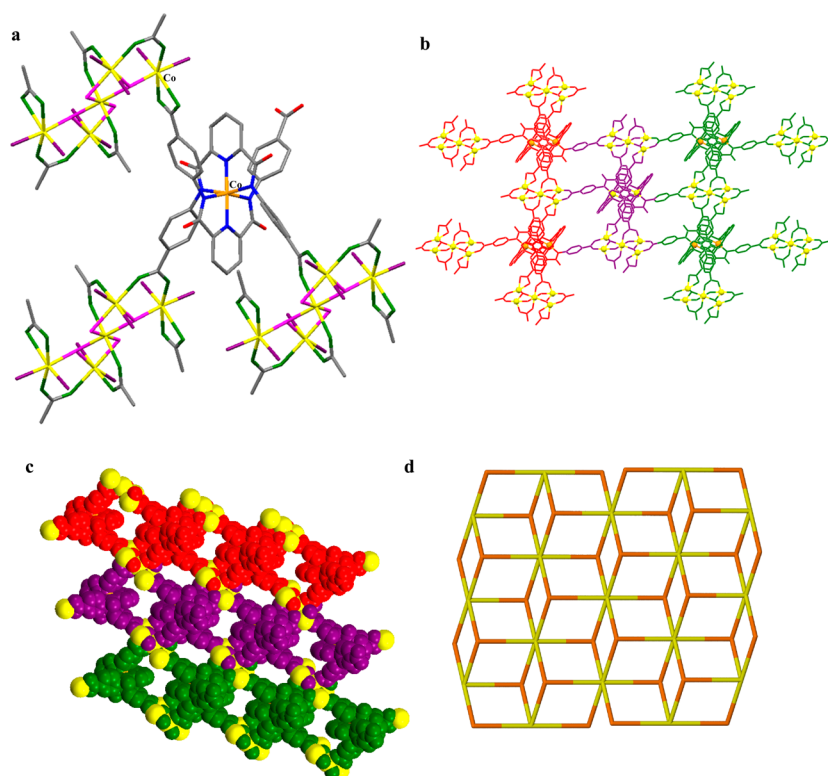
Figure 3. (a) Stick representation of a selected part of the crystal structure of network **5**. Color code: orange, Co; yellow, Co (secondary metal ions); blue, N; green, O$_{carboxylate}$; purple, O$_{water}$; magenta, O$_{bridging\ water/hydroxide}$; red, O$_{amide}$; gray, C. (b) Packing diagram in a view along the *b* axis. (c) Space-filling view along the *c* axis showing pores and channels in the structure of network **5**; coordinated water molecules are omitted for clarity to show accessible Co^{2+} ions (yellow spheres). (d) Topological representation of the network. Color code: orange, central Co^{3+} core as the node; yellow, Co$_5$ cluster as the node.

Figure 4. (a) Stick representation of a selected part of the crystal structure of network **6**. Color code: orange, Co; yellow, Co (secondary metal ions); blue, N; green, O$_{carboxylate}$; purple, O$_{water}$; magenta, O$_{bridging\ water}$; red, O$_{amide}$; gray, C. (b) Packing diagram in a view along the *b* axis. (c) Topological representation of the network. Color code: orange, central Co^{3+} core as the node; yellow, Co$_2$ cluster as the node.
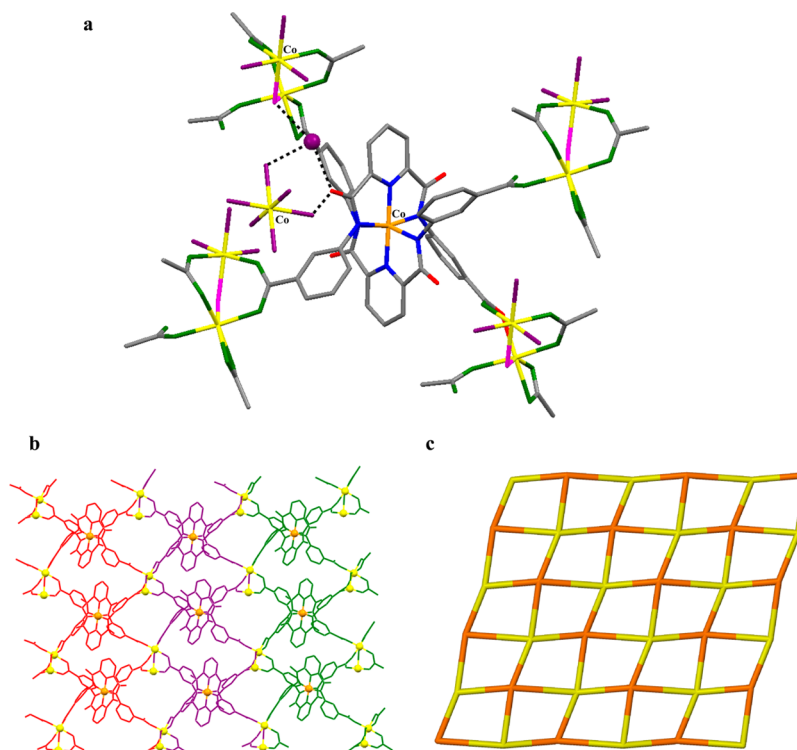
Table 1. Selected Ranges for the Bond Distances (Angstroms) Observed for Networks 3–6[a]

bond lengths	3	4	5	6
$Co1-N_{pyridine}$	1.844(4)–1.858(4)	1.866(9)–1.868(8)	1.860(6)–1.861(4)	1.850(6)–1.858(6)
$Co1-N_{amide}$	1.941(4)–1.945(4)	1.931(10)–1.967(10)	1.951(5)–1.970(5)	1.926(6)–1.960(7)
$M-O_{carboxylate}$	2.141(4)–2.193(4)	2.099(9)–2.461(10)	2.026(4)–2.143(7)	2.016(7)–2.187(6)
$M-O_{amide}$	2.142(4)			
$M-O_{hydoxide}$		2.261(10)–2.273(8)	2.035(4)–2.088(4)	2.177(5)–2.178(5)
$M-O_{bridging\ water}$			2.161(4)–2.200(4)	
$M-O_{terminal\ water}$	2.163(4)–2.222(5)	2.189(10)–2.217(10)	2.084(4)–2.145(4)	2.088(7)–2.145(8)

[a]Where M = Mn^{2+} in networks **3** and **4** and Co^{2+} in networks **5** and **6**.

metal ions is ligated with two $O_{carboxylate}$ atoms, one bridging hydroxide, and three water molecules, while coordination sites for the second metal ion are satisfied by five $O_{carboxylate}$ and a bridging hydroxide group. Notably, in both cases, the third metal is present as $\{M(H_2O)_6\}^{2+}$ cluster in the crystal lattice.[25f] Such a $\{M(H_2O)_6\}^{2+}$ cluster is held in a network lattice by the operation of assorted H-bonds between M-bound water molecules, O_{amide} atoms, and lattice water molecules. Noticeably, when the grinded sample of either network **4** or **6** is suspended in various solvents the $\{M(H_2O)_6\}^{2+}$ cluster does not come out from the crystal lattice.[25f] Further, no exchange was observed when the powdered sample is suspended in a solvent containing other divalent or trivalent metal ions. These experiments suggest the stable nature of $\{M(H_2O)_6\}^{2+}$ cluster within the network and the requirement of charge balance is the primary driving force for their presence in a lattice. Both networks **4** and **6** offer smaller pores with 8.79 × 8.34 and 8.06 × 7.98 Å² cross-sectional area, respectively.

Network Topology. The topology of all four coordination networks has been examined in more detail using the TOPOS software.[33,34] Although all four networks suggest a similar architecture, they are topologically distinct.[35] The networks offer secondary building units (SBUs)[36a,b] that are composed of secondary Mn^{2+} or Co^{2+} ions coordinated by a certain number of arylcarboxylate fragments: $Mn(COO)_2$ (**3**), $Mn_2(COO)_4$ (**4**), $Co_5(COO)_6$ (**5**), and $Co_2(COO)_4$ (**6**). In all cases, such SBUs expand through tetratopic Co^{3+}-based metalloligands that may be considered as nodes.[36] Both networks **4** and **6**, generated via Co^{3+}-based metalloligands appended with m-arylcarboxylate groups, are topologically identical wherein $Mn_2(COO)_4$ (**4**) or $Co_2(COO)_4$ (**6**) SBUs serve as the 4-connected cluster nodes[37] by linking to four Co^{3+}-based metalloligands. Similarly, every Co^{3+}-based metalloligand can also be viewed as a 4-connected node which in turn links to four $Mn_2(COO)_4$ or $Co_2(COO)_4$ SBUs resulting in a (4,4)-connected network parallel to the ac plane (Figures 2c and 4c).[38] After applying the TOPOS simplification process the resulting networks of **4** and **6** can be specified as the sql/Shubnikov tetragonal plane nets with point symbol $\{4^4.6^2\}$.[39] Interestingly, network **5**, generated via Co^{3+}-based metalloligand appended with p-arylcarboxylate groups, is topologically distinct from the other two networks, **4** and **6**. This network can be topologically interpreted as a (3,6)-connected network parallel to the ab plane wherein $Co_5(COO)_6$-based SBUs serve as the 6-connected cluster nodes,[37] while every metalloligand stands for a 3-connected node (Figure 3d). The TOPOS analysis of network **5** provides the kgd/Shubnikov plane net topology with the point symbol $\{4^3\}_2\{4^6.6^6.8^3\}$.[40]

Voids and Pores. Notably, all four networks show solvent-accessible voids (SAVs) of different volumes, and considerable differences were noted between the networks created by p-

versus m-arylcarboxylate groups-based metalloligands. For example, crystal structures of networks **3** and **5**, with p-arylcarboxylate groups, show SAVs corresponding to ca. 22.6% and 23.7% of the unit cell volume, respectively. On the other hand, networks **4** and **6** (with m-arylcarboxylate groups) exhibited small or negligible SAVs. Such a striking difference is due to a symmetrical nature of bonding between meta-appended arylcarboxylate groups and that of secondary metal ions in case of networks **4** and **6** that has resulted in little voids in the lattice. In fact, our earlier $\{Co^{3+}-Zn^{2+}\}$ and $\{Co^{3+}-Cd^{2+}\}$ coordination networks with meta-appended arylcarboxylate groups also showed very small or negligible SAVs compared to large SAVs exhibited by networks with para-appended arylcarboxylate groups.[25e,f] Furthermore, a very similar H-bonding-based packing was observed for the Co^{3+}-based metalloligands appended with m-arylcarboxylic acid groups offering very small or essentially negligible SAVs.[23b]

All four networks exhibit well-defined pores and channels within the network. Such pores and channels were found to contain lattice water molecules which were held together by weak H-bonding interactions. Interestingly, networks **3** and **5**, with p-arylcarboxylate groups, offered pores with larger cross sections of 19.96 × 18.50 Å² (for **3**) and 11.15 × 7.46 and 11.83 × 11.69 Å² (for **5**). Networks **4** and **6** with m-arylcarboxylate fragments displayed smaller pores of 8.79 × 8.34 and 8.06 × 7.98 Å² cross-section area, respectively. Therefore, it could be concluded that p-arylcarboxylate groups produced elongated networks that offered wider pores and large SAVs. Importantly, such structural features are expected to enhance the substrate and/or reagent accessibility. In addition, all four networks showed an orderly arrangement of secondary metal ions within the crystalline architectures. Importantly, such secondary metal ions are not only oxidation sensitive in nature but also coordinated with labile water molecules. It was therefore presumed that the suitable substrates may interact with such metal sites and replace the labile water molecules without altering the network topology, and such a situation may assist in possible catalysis.

Thermal Properties. It is a well-known fact that the heterogeneous catalytic applications depend on the thermal stability of coordination networks; therefore, thermal gravimetric analysis (TGA) and differential scanning calorimetric (DSC) analyses were performed on all four networks (Figures S11–S14, Supporting Information). All four networks displayed similar thermal profiles due to a comparable network topology and coordination environment. For all four networks, the first weight loss was observed in the temperature range of 25–90 °C corresponding to loss of coordinated as well as lattice water molecules. For all four networks, the observed weight losses were in close match to that of calculated ones for the liberation of both coordinated as well as lattice water

molecules. DSC studies supported the TGA finding by displaying a broad feature in the exothermic region for the loss of water molecules. The thermal analyses further exhibit that all four networks are stable after the loss of water molecules as no additional weight loss was noted up to ca. 350 °C.

Exchange and Inclusion Properties. In order to evaluate possible diffusion of substrates and/or reagents through the pores and channels of networks **4−6**, sorption, exchange, and inclusion studies were carried out. The N_2 sorption studies at 77 K for all four networks showed small uptake with low Langmuir and BET surface area. Notably, our earlier metal-loligand-based networks[25a−c,e,f] as well as related materials in the literature have also displayed similar low-sorption behavior.[41] We, therefore, attempted to discern possible exchange as well as inclusion of reagents and substrates within the pores and channels of the present networks.[42]

One of the significant challenges was to evaluate that the coordinated water molecules are labile in nature so that the substrates and/or reagents are able to replace them. We, therefore, performed solvent exchange reactions using D_2O and alcohol vapors. For such experiments, powdered networks were first heated at 150 °C under vacuum in order to remove lattice as well as coordinated water molecules followed by allowing samples to equilibrate in a sealed environment of D_2O vapors. Such an experiment resulted in clean exchange of H_2O by D_2O, and the ν_{O-D} stretches were observed at 2480−2490 cm^{-1} with a shift of ca. 900 cm^{-1} from ν_{O-H} stretches (Figures S15−S18, Supporting Information). In order to confirm that the networks retain their structural integrity and crystallinity during the solvent removal and D_2O exchange experiments, all four networks were investigated by the XRPD studies after the D_2O exchange. Notably, all four networks retain their structural integrity and crystallinity as revealed by the XRPD patterns. Importantly, several reflections displayed broad features with minor shifts as a result of D_2O exchange which further support our exchange assumption (Figures S19−S22, Supporting Information).

We further attempted to understand if coordinated water molecules could also be exchanged with few other similar ligands. Thus, exchange studies were carried out using network **3** as a representative case with a few alcohols, such as CH_3OH, C_2H_5OH, C_3H_7OH, and *tert*-BuOH (Figures S23−S27, Supporting Information). As an illustration, ν_{O-Me} stretch for the exchanged MeOH was clearly evident at 1060 cm^{-1}. It was observed that the coordinated/lattice water molecules were replaced with alcohol in the following order: $CH_3OH \gg C_2H_5OH \gg C_3H_7OH \approx$ *tert*-BuOH. Importantly, both D_2O and alcohol exchange experiments strongly suggest the propensity of exchange of the coordinated/lattice water molecules by the suitable solvents/ligands where the size of the alcohol appears to be a limiting factor.

To further investigate the feasibility of possible diffusion of reagents and/or substrates through the pores and channels of the networks, FTIR and ^1H NMR spectral and XRPD studies were carried out for the networks. Thus, when powdered networks **3−6** were impregnated with a CH_2Cl_2 solution containing a few substrates (4-methoxystyrene, 4-methylstyrene, 4-*tert*-butylstyrene, cyclohexene, and *cis*-stilbene), FTIR spectra (Figures S28−S32, Supporting Information) displayed noticeable differences[42] when compared to neat samples whereas XRPD patterns (Figures S33 and S34, Supporting Information) ascertained the structural integrity of the

networks during such studies. For example, $\nu_{C=C}$ stretches for the impregnated substrates were red shifted by 8−10 cm^{-1}. In addition, diffusion and probable inclusion of such substrates also caused noticeable perturbation to the ν_{O-H} stretches of the coordinated/lattice water molecules (cf. Figures S28−S32, Supporting Information).

We finally carried out a ^1H NMR spectral-based inclusion experiment to ascertain the coexistence of both substrate and reagent within the porous network and their reaction within the confined environment. Therefore, styrene was selected as a model substrate using TBHP as an oxidizing agent and network **3** as a representative catalyst. Network **3** was impregnated with a 1:3 mixture of styrene and TBHP and investigated after digesting the sample using DCl and extracting the products into EtOAc at the following intervals: 1, 2, 4, 5, and finally at 6 h. The ^1H NMR spectral results at 2 h display the peaks for substrate (styrene) as well as the epoxidation product (styrene oxide) (Figure S35, Supporting Information). Notably, after 6 h, the peaks corresponding to substrate were negligible while product formation was almost quantitative, whereas the reaction showed ca. 70% completion after 4 h. Such an experiment provides additional evidence that catalysis is possibly occurring within the porous network and the reagents not only have diffused but also reacted within the porous network.

Application of {Co^{3+}−Mn^{2+}} and {Co^{3+}−Co^{2+}} Networks in Olefin Epoxidation Reactions. Activation of molecular oxygen is an important process in biology, chemistry, and industry.[13,14,21,22] Such an activation ranges from the oxidation of C−H bonds, hydroxylation, epoxidation, and oxidation of heteroatom-based substrates.[13] Significant efforts have been made to generate simple yet efficient methods to activate molecular oxygen.[21] Learning from the biological systems, metalloporphyrins,[17a] metallophthalocyanins,[17b] and Schiff-base-based complexes[18] have been effectively developed but the activation process largely remains limited to homogeneous reactions. In this regard, efforts have also been made to heterogenize the molecular components in order to achieve heterogeneous activation of molecular oxygen.[20] Out of assorted heterogeneous catalysts, coordination networks including metal−organic frameworks (MOFs) have shown remarkable results.[10,11] Our coordination networks offer interesting oxidative catalytic perspectives considering the following points: (i) all four networks allow unhindered diffusion of substrates and/or reagents, (ii) secondary metal ions are coordinated by labile water molecules, (iii) secondary metal ions are redox active and therefore likely to support oxidation reactions, (iv) secondary metal ions line both external as well as internal surfaces and are likely to enhance the interaction with substrates and reagents, and (v) all four networks are thermally stable up to 350 °C. We selected epoxidation of assorted olefins due to the importance of epoxides as the key starting materials for a wide variety of industrial and chemical applications.[14,15]
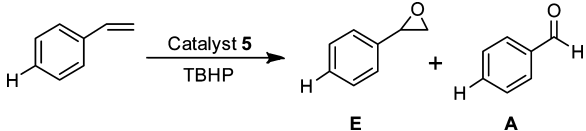
We noted that any of the four networks could act as a catalyst for the epoxidation of styrene or substituted styrenes using TBHP as an oxidizing agent. We, however, performed a series of control experiments in order to optimize the reaction conditions for a better catalytic efficiency and to avoid the formation of undesirable side product(s). Of course, one of the initial experiments substantiated that networks **3−6** are essential in oxidation catalysis as without them only traces of products were noticed in most cases (Table S6, Supporting

Information; entries 1−19). The control and optimization experiments are discussed in the following sections.

Oxidizing Agent. In order to find out the best oxidizing agent, we screened the following reagents: H_2O_2, TBHP (in decane), TBHP (in water), PhIO, *N*-methyl-morpholine-*N*-oxide (NMO), trimethylamine-*N*-oxide (TMO), *m*-chloroperbenzoic acid, and NaOCl. Notably, only TBHP was successful, while other oxidizing agents did not result in the oxidation of styrene (model substrate) or led to partial decomposition of the networks. Interestingly, all four networks caused fast disproportionation of *m*-chloroperbenzoic acid, resulting in vigorous generation of molecular oxygen. Importantly with TBHP in decane, the product yield of styrene oxide was almost quantitative with a very small amount of benzaldehyde, whereas TBHP in water resulted in poor oxidation. It appears that the presence of excess water had a detrimental effect on the catalytic performance of networks. We believe that additional water molecules possibly block the catalytic secondary metal ions (also see next section, solvent). To prove such a fact, when epoxidation of styrene was carried out in the presence of molecular sieves, the reaction could be quantitatively completed within 2 h rather than 4 h without sieves. Such an experiment convincingly suggests that catalysis is occurring via displacement of the coordinated water molecule(s) by the substrate, and excess water potentially hampers such a vital step.

Solvent. To evaluate the effect of solvent in the catalytic oxidation of olefins, styrene was selected as the model substrate in the presence of catalyst **5** while screening various solvents (Table 2). Styrene oxide was the major product in most cases,

Table 2. Epoxidation of Styrene with TBHP in the Presence of Catalyst 5: Effect of Solvents and Additives

entry[a]	substrate	solvent/additive	yield (%)[b]	
			E	A
1	styrene	CH_3CH_2OH	80	20
2	styrene	CH_3OH	74	26
3	styrene	THF	60	40
4	styrene	CH_3CN	60	40
5	styrene	DMF	60	20
6	styrene	dioxane	24	67
7[c]	styrene	pyridine	67	15
8[c]	styrene	*t*-BuOH	44	14
9[c]	styrene	NaOAc	53	20
10[c]	styrene	morpholine	67	14

[a]Conditions: Network **5** as catalyst (2 mol %); 4 h stirring at 50 °C. [b]Yield was calculated from gas chromatography. [c]Under solvent-free conditions.

while benzaldehyde was also produced as the undesirable byproduct in varying amounts. The highest yield of styrene oxide (80%) was obtained in the case of C_2H_5OH (entry 1) and lowest (24%) in dioxane (entry 6), whereas MeOH, THF, MeCN, and DMF provided moderate yields. The results reveal that the oxidation of styrene to styrene oxide is higher in highly polar solvents than that of less polar solvents. Furthermore, less polar solvents enhanced the yield of benzaldehyde (67% in the case of dioxane; entry 6). We reasoned that the better solvation

effect of a polar solvent plays a crucial role in the displacement of the coordinated water molecule(s) from the secondary metals within the network and enhances the olefin accessibility, thus resulting in better conversion. Subsequent control experiments, however, established that the oxidation of styrene to styrene oxide is maximum (92−95%; Table 3) under the solvent-free reaction conditions with all four networks with minimum production of benzaldehyde. This is probably due to a better interaction between catalytic sites and the substrate when its concentration is high under the solvent-free condition. In fact, TBHP in decane (with negligible coordinating ability) acted as the best oxidant, while TBHP in water (with very high coordinating ability) only poorly functioned. Such an observation further strengthens that the solvent-free reaction conditions are the best for epoxidation with the present networks.

Additive. In porphyrin- and salen-based oxidation chemistry, the presence of additive(s) plays a significant and sometime decisive role in olefin epoxidation reactions.[43] We, therefore, attempted to understand the role played by the additives. Importantly, there was no improvement in the oxidation of styrene to styrene oxide when an additive was added during the course of the reaction. For example, when pyridine was added as an additive, the yield of the epoxide is 67% while the byproduct benzaldehyde is 15% (entry 7, Table 2). However, with *t*-BuOH, the yield of the styrene oxide dropped to 44% (entry 8), whereas in the case of NaOAc and morpholine, only 53% and 67% epoxidation took place (entries 9 and 10, Table 2). Further, the presence of additives did not suppress the formation of benzaldehyde. We speculate that the presence of a better coordinating moiety (i.e., additive) rather blocks the labile sites on secondary metal ions crucial for subsequent catalysis. Therefore, it could be concluded that additive(s) do not play any major role with our catalytic networks and oxidation of styrene to styrene oxide is better in the absence of any additive (92−95%, Table 3).

Presence of O_2. We further investigated the effect of aerobic conditions in the oxidation of styrene (Table S7, Supporting Information). Notably, large amounts of benzaldehyde as well as benzoic acid were formed as the byproducts along with the desired product, styrene oxide. It is clear that the presence of molecular oxygen resulted in free-radical-based oxidation of styrene, resulting in the formation of benzaldehyde as well as benzoic acid.[14e] In fact, network **4** predominantly produced benzoic acid (70%) in addition to benzaldehyde (20%) and styrene oxide (10%). Interestingly, out of four networks, **3** was efficiently able to oxidize styrene to styrene oxide in 64% yield even under aerobic reaction condition (entry 1; Table S7, Supporting Information).

Catalyst Loading. We also made efforts to understand the optimal loading of catalyst in order to efficiently carry out the epoxidation reactions. For such a purpose, catalyst loadings of 0.5, 1, 2, and 5 mol % were used for the oxidation of styrene using TBHP. The product yield of styrene oxide varied in the anticipated manner in the following order: 0.5 mol % (50) < 1 mol % (60) < 2 mol % (92) < 5 mol % (95). As the results were closely similar to 2 and 5 mol % catalyst loading, we decided to use only 2 mol % in an attempt to minimize the use of catalyst.

Reaction Time. To evaluate the effect of reaction time on epoxide yield, we performed time-dependent oxidation of styrene using TBHP with catalyst **5** under the solvent-free reaction conditions (Figure S36 and Table S8, Supporting

Table 3. Epoxidation of Substituted Styrenes and Other Olefins with TBHP in the Presence of Catalyst 3, 4, 5, or 6 under Solvent-Free Conditions

| | | yield (%)[b] | | | | | | | |
| | | 3 | | 4 | | 5 | | 6 | |
entry[a]	R/substrate	E	A	E	A	E	A	E	A
1	H	94	5	92	6	95	5	93	6
2	4-Me	92	8	93	7	92	7	95	5
3	4-OMe	92	6	92	7	92	6	92	6
4	4-Cl	95	5	94	6	94	6	95	5
5	4-C(CH$_3$)$_3$	78	8	69	7	75	8	83	10
6	1-vinylnaphthalene	55	11	52	9	59	8	68	10
7	2-vinylnaphthalene	60	12	59	10	74	10	70	12
8	9-vinylanthracene	26	4	38	5	22	3	24	6
9	cis-stilbene	26	4	27	4	26	3	30	5
10	trans-stilbene	94	5	93	7	92	6	94	5

[a]Conditions: Networks 3−6 as catalyst (2 mol %); 4 h stirring at 50 °C. [b]Yield was calculated from gas chromatography.

Table 4. Epoxidation of Assorted Cyclic Olefins with TBHP in the Presence of Catalyst 3, 4, 5, or 6 under Solvent-Free Conditions

| | | Yield (%)[b] | | | | | | | | | | |
| | | 3 | | | 4 | | | 5 | | | 6 | | |
Entry[a]	Substrate	E	K-1	K-2	E	K-1	K-2	E	K-1	K-2	E	K-1	K-2
1		95	5	---	95	5	---	94	6	---	96	4	---
2		73	---	27	72	---	28	82	---	18	80	---	20
3		84	16	---	85	15	---	80	20	---	82	18	---
4		74	26	---	75	25	---	76	24	---	78	20	---
5		100	---	---	100	---	---	100	---	---	100	---	---

[a]Conditions: Networks 3−6 as catalyst (2-mol %); 4 h stirring at 50 °C. [b]Yield was calculated from the gas chromatography.

Information). As expected, the yield of the epoxide is directly proportional to the reaction time, reaching the saturation after 4 h. The quantitative product conversion (95% styrene oxide; 5% benzaldehyde) was observed after 4 h, whereas only 20% conversion was noted after 1 h (Table S8, Supporting Information, compare entries 1 and 6).

Reaction Temperature. To assess the optimal reaction temperature, epoxidation of styrene was carried out using network 5 at the following temperatures: 25, 50, 75, and 100 °C. With 2 mol % catalyst loading, the best performance was achieved at 50 °C while the epoxidation remained incomplete at 25 °C. Notably, higher temperature resulted in the large production of undesirable benzaldehyde.

Epoxidation Reactions. The aforementioned control and optimization experiments allowed us to explore epoxidation reactions of assorted substrates, and the results are presented in Tables 3−5. In a typical epoxidation reaction, olefin and TBHP were reacted in a 1:3 ratio in the presence of 2 mol % of catalyst (networks 3, 4, 5 or 6) at 50 °C under the solvent-free reaction conditions. Under these conditions, a smooth reaction took place and the desired product, epoxide, was formed in good yield along with a small amount of byproduct (respective aldehyde). All four networks produced 92−95% styrene oxide in addition to 5−6% of benzaldehyde (entry 1; Table 3). To evaluate the impact of the electronic effect on the epoxidation of olefin, several para-substituted styrenes were used. Notably,

Table 5. Epoxidation of Assorted Linear Olefins with TBHP in the Presence of Catalyst 3, 4, 5, or 6 under Solvent-Free Conditions

Entry[a]	Substrate	3		4		5		6	
		E	K	E	K	E	K	E	K
1		74	26	74	26	76	23	80	20
2		73	27	82	18	66	34	79	20
3		58	42	59	41	58	42	64	35
4		98	2	97	3	98	2	99	---

Yield (%)[b] header spans columns 3, 4, 5, 6.

[a]Conditions: Networks **3–6** as catalyst (2 mol %); 4 h stirring at 50 °C. [b]Yield was calculated from the gas chromatography.

both electron-rich as well as electron-deficient styrenes were equally effective with all four networks (92–95% yield; entries 1–4; Table 3). However, in the case of 4-*tert*-butyl-1-vinylbenzene, the yield is dropped to 69–83% (entry 5; Table 3), probably due to the steric hindrance of the *tert*-butyl group which may have restricted its accessibility to the catalytic sites. A similar observation was noted for the diffusion and exchange studies using *tert*-butyl alcohol. The influence of steric hindrance is further supported by the epoxidation of sterically demanding substrates, such as 1-vinylnaphthalene, 2-vinyl-napthalene, and 9-vinyl anthracene. In these cases, substrate-size-dependent catalysis was observed. For network **6**, the conversion decreased in order of styrene (93%) > 4-*tert*-butyl-1-vinylbenzene (83%) > 1-vinylnaphthalene (68%) ≈ 2-vinylnapthalene (70%) > 9-vinylanthracene (24%) in line with their sizes:[44] styrene (7.00 × 8.45 Å^2), 4-*tert*-butyl-1-vinylbenzene (7.00 × 9.93 Å^2), 1-vinylnapthalene (7.00 × 8.81 Å^2), 2-vinylnaphthalene (7.00 × 10.37 Å^2), 9-vinylanthracene (8.42 × 10.34 Å^2). A somewhat similar trend was observed for the remaining networks. We, therefore, tentatively suggest that the epoxidations are inversely proportional to the molecular size of the substrates and substrate accessibility to the Mn^{2+} or Co^{2+} sites controls the catalysis outcome.

In the epoxidation of *cis*- and *trans*-stilbene, stilbene oxide was the major product along with a small amount of benzaldehyde. Notably, with our catalytic networks there was no evidence for the formation of benzil as frequently reported in the literature.[45] The epoxidation of *cis*-stilbene was poor and afforded only 26–30% product yield (entry 9; Table 3), while *trans*-stilbene was oxidized in excellent yield, ranging between 92% and 94% (entry 10; Table 3). It is believed that cis to trans isomerization is one of the major factors for the observed stereoselectivity and therefore poor oxidation of *cis*-stilbene. Notably, only a trace amount of benzaldehyde was produced both in *cis*- and in *trans*-stilbene epoxidation reactions.

The applicability of the catalytic networks was further extended to the epoxidation of assorted cyclic olefins. All cyclic olefins were oxidized in good to excellent yields (entries 1–5; Table 4). In most cases, the amount of undesirable keto products, K-1 and K-2, was limited to small quantities. Interestingly, under identical reaction conditions, 1-methyl-cyclohexene showed 100% epoxidation with all four networks (entry 5). This is most probably due to the presence of a methyl group, which shows a +I effect and makes 1-

methylcyclohexene a more electron-rich olefin. Cyclopentene displayed a greater reactivity due to a smaller ring size and easy accessibility (94–96%) than the sterically demanding cyclo-octene which produces 74–78% of the corresponding epoxide (entries 1 and 4). Cyclohexene and cycloheptene also exhibited similar transformations (entries 2 and 3). It is important to note that in all epoxidation reactions, except 1-methylcyclohex-ene, the allylic oxidation product (-one; entries 1, 3, and 4; dione, entry 2) was also obtained (5–28%) as the byproduct. The formation of allylic product suggests the involvement of a radical mechanism in the epoxidation of cyclic olefins (see mechanistic insights). Notably, the quantity of allylic product is quite small for the conformationally rigid molecules, such as cyclopentene and 1-methylcyclohexene, but large for the flexible cyclic olefins as noted for 6-, 7-, and 8-membered rings.

It is generally assumed that the oxidation of terminal alkenes is difficult due to the presence of an electron-deficient double bond. Importantly, our catalytic networks were equally effective in the epoxidation of terminal alkenes (Table 5). All four networks were able to oxidize 1-hexene (74–80%), 1-heptene (66–82%), 1-nonene (58–64%), and 1-decene (>97%) effortlessly. Interestingly, the yield of the epoxide was almost quantitative for 1-decene but quite low for 1-nonene. The reason for this behavior is probably related to the optimal orientation of the substrate within the network channel in the absence of other limiting parameters.

Leaching and Control Experiments. In order to ascertain whether the secondary metal ions are leaching out or not, after 3 h of epoxidation, solid networks were filtered off and the reaction was allowed to continue. As illustrated in Figure 5 using network **5** as a representative case, there was practically no epoxidation after filtering off network **5**. Subsequently, network **5** was readded after a gap of 2 h, which immediately caused the epoxidation of styrene. An overall reaction profile displays that the removal of network **5** practically ceases the epoxidation while readding the filtered network **5** to the reaction mixture restarts the epoxidation. This simple test establishes the *true* heterogeneous catalytic behavior of network **5**. Further, control experiments of using metalloligands **1** or **2** or metal salts (CoCl$_2$, MnCl$_2$, Co(OAc)$_2$, Mn(OAc)$_2$, or Mn(OAc)$_3$) as the catalysts did not result in any product formation. To confirm that the secondary metal ions, Co(II) and Mn(II), are indeed required for the epoxidation reactions, we tested our earlier Zn(II)- and Cd(II)-based networks[25e,f]
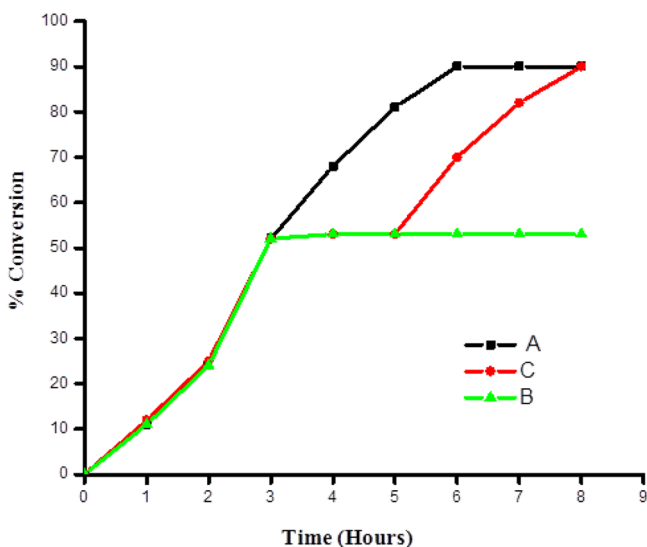
Figure 5. (A) Epoxidation of styrene with TBHP in the presence of network **5** showing maximum oxidation at 6 h. (B) Catalyst was filtered after 3 h, and epoxidation was ceased. (C) Catalyst was readded after a gap of 2 h, and maximum epoxidation was observed after 3 h. In all cases, the yield was calculated using gas chromatography.

with identical metalloligands **1** and **2** for the epoxidation reactions. Satisfyingly, negligible epoxidations (<5%) were observed for such networks, which we believe are due to surface-based activation of TBHP. Collectively, such experiments substantiate that the soluble and/or catalytic active species are not leached out from the present networks under the employed reaction conditions and networks **3−6** are acting as genuine heterogeneous catalysts.

Recyclability Experiments. The solid heterogeneous networks **3−6** can readily be separated from the reaction mixture by simple filtration: a feature unique to the heterogeneous and/or solid immobilized catalysts that conveniently allows for studies of recyclability of the catalysts. Indeed, all four networks are recyclable under the reaction conditions up to several cycles, and Table S9, Supporting Information, displays results with two representative networks. It was noted that the amount of aldehyde was slightly increased with reused networks when compared to pristine samples. However, all four networks retain their crystallinity, reactivity,

and selectivity throughout these numbers of cycles. Notably, there was no special requirement of any purification or regeneration for any of the networks, as they can be simply filtered, washed with wet methanol, and dried at room temperature and were ready for reuse. The FTIR spectra and XRPD patterns authenticate that the crystallinity and structural integrity of the recovered networks is preserved after the catalytic reaction. A comparison of XRPD patterns of the pristine samples to that of recovered networks unambiguously supports this observation (Figures S37−S40, Supporting Information).

Mechanistic Insights. The epoxidation reactions are typically believed to operate either through a radical pathway or via concerted metal−oxo species.[46] In order to ascertain which one, we decided to carry out epoxidations in the presence of potential radical scavengers such as substituted phenols. Importantly, in the presence of 2,4-di-*tert*-butylphenol, 2,6-di-*tert*-butylphenol, and 2,4,6-tri*tert*-butylphenol, epoxidation was completely quenched whereas oxidized products (diquinones 5−25%) and/or carbon−carbon coupled products (2−10%) from the substituted phenols were observed. These experiments convincingly suggest that the epoxidation proceeds via a radical-based mechanism.[14e,46−48] On the other hand, the same reaction in the presence of dioxygen displayed the formation of benzoic acid and aldehyde products as a result of dioxygen involvement (see Table S7, Supporting Information). Thus, the proposed reaction mechanism is shown in Scheme 2. First, reaction between the secondary M^{n+} ion and TBHP takes place to form a M^{n+1}−peroxy adduct. The M^{n+1}−peroxy adduct then releases a *tert*-butoxy radical and regenerates M^{n+} ion. This is followed by a reaction between *tert*-butoxy radical and olefin to form a *tert*-butoxperoxy species that further undergoes migration of oxygen to form the epoxide as the product[49] and *tert*-BuOH as the byproduct.[50] Furthermore, possible involvement of dioxygen or *tert*-butoxy radicals with the *tert*-butoxperoxy species will result in some acid and aldehyde byproducts.

■ CONCLUSION

To summarize, we synthesized {Co^{3+}−Mn^{2+}} and {Co^{3+}−Co^{2+}} heterobimetallic coordination networks using Co^{3+}-based metalloligands appended with arylcarboxylate groups as the building blocks. We successfully demonstrated that the immobilized catalytically active secondary Mn^{2+} and Co^{2+} ions efficiently carry out epoxidation of a number of olefins without

Scheme 2. Proposed Reaction Mechanism for the Epoxidation Reaction Catalyzed by Networks 3−6[a]
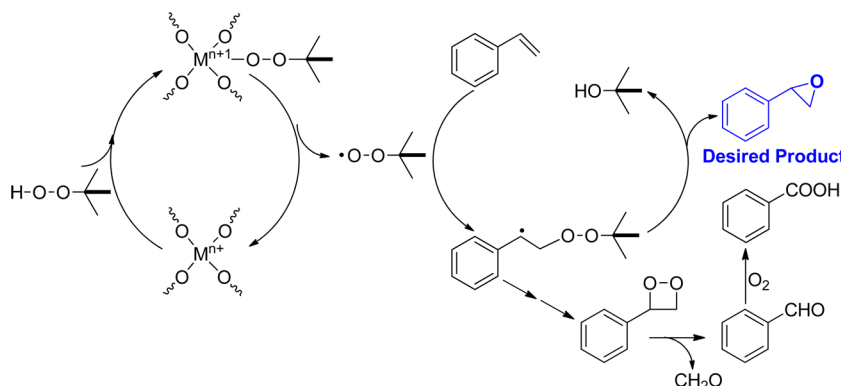
[a]M stands for Mn^{2+} ions in **3** and **4** and Co^{2+} ions in **5** and **6**, respectively.

any requirement of solvent or additive. The heterogeneous networks demonstrate outstanding structural stability and therefore good reusability. These examples display great promise in the development of crystalline coordination networks for catalytic applications.

■ ASSOCIATED CONTENT

Ⓢ Supporting Information

X-ray crystallographic data for networks **3−6** in CIF format; figures for the diffuse-reflectance absorption spectra, XRPD patterns, crystal structures, TGA-DSC plots, FTIR spectra, NMR spectra; tables for X-ray data collection, bonding parameters, catalysis, reusability, and size calculations of a few substrates and/or reagents. This material is available free of charge via the Internet at http://pubs.acs.org.

■ AUTHOR INFORMATION

Corresponding Author
*Fax: +91-11-2766 6605. E-mail: rgupta@chemistry.du.ac.in.
Author Contributions
†Girijesh Kumar and Gulshan Kumar have contributed equally.
Notes
The authors declare no competing financial interest.

■ ACKNOWLEDGMENTS

■ REFERENCES

(1) (a) Zhou, H.-C.; Kitagawa, S. *Chem. Soc. Rev.* **2014**, *43*, 5415−5418. (b) Cook, T. R.; Zheng, Y.-R.; Stang, P. J. *Chem. Rev.* **2013**, *113*, 734−777. (c) Chakrabarty, R.; Mukherjee, P. S.; Stang, P. J. *Chem. Rev.* **2011**, *111*, 6810−6918. (d) Li, M.; Li, D.; O'Keeffe, M.; Yaghi, O. M. *Chem. Rev.* **2014**, *114*, 1343−1370. (e) O'Keeffe, M.; Yaghi, O. M. *Chem. Rev.* **2012**, *112*, 675−702. (e) Fujita, M.; Tominaga, M.; Hori, A.; Therrien, B. *Acc. Chem. Res.* **2005**, *38*, 371−380.

(2) (a) Barea, E.; Montoro, C.; Navarro, *Chem. Soc. Rev.* **2014**, *43*, 5419−5430. (b) Canivet, J.; Fateeva, A.; Guo, Y.; Coasne, B.; Farrusseng, D. *Chem. Soc. Rev.* **2014**, *43*, 5594−5617. (c) Suh, M. P.; Park, H. J.; Prasad, T. K.; Lim, D. W. *Chem. Rev.* **2012**, *112*, 782−835. (d) Sumida, K.; Rogow, D. L.; Mason, J. A.; McDonald, T. M.; Bloch, E. D.; Herm, Z. R.; Bae, T. H.; Long, J. R. *Chem. Rev.* **2012**, *112*, 724−781. (e) Wenger, O. S. *Chem. Rev.* **2013**, *113*, 3686−3733. (f) Murray, L. J.; Dinca, M.; Long, J. R. *Chem. Soc. Rev.* **2009**, *38*, 1294−1314. (g) He, Y.; Zhou, W.; Qian, G.; Chen, B. *Chem. Soc. Rev.* **2014**, *43*, 5657−5678.

(3) (a) de Voorde, B. V.; Bueken, B.; Denayer, J.; Vos, D. D. *Chem. Soc. Rev.* **2014**, *43*, 5766−5788. (b) Li, J. R.; Sculley, J.; Zhou, H. C. *Chem. Rev.* **2012**, *112*, 869−932. (c) Li, J. R.; Kuppler, R. J.; Zhou, H. C. *Chem. Soc. Rev.* **2009**, *38*, 1477−1504. (d) Li, B.; Wang, H.; Chen, B. *Chem. Asian. J.* **2014**, *9*, 1474−1498.

(4) (a) Hu, Z.; Deibert, B. J.; Li, J. *Chem. Soc. Rev.* **2014**, *43*, 5815−5840. (b) Kreno, L. E.; Leong, K.; Farha, O. K.; Allendorf, M.; Duyne, R. P. V.; Hupp, J. T. *Chem. Rev.* **2012**, *112*, 1105−1125. (c) Potyrailo, R. A.; Surman, C.; Nagraj, N.; Burns, A. *Chem. Rev.* **2011**, *111*, 7315−7354.

(5) (A) Brozek, C. K.; Dinca, M. *Chem. Soc. Rev.* **2014**, *43*, 5456−5467. (b) Ramaswamy, P.; Wong, N. E.; Shimizu, G. K. H. *Chem. Soc. Rev.* **2014**, *43*, 5913−5932.

(6) Qui, S.; Xue, M.; Zhu, G. *Chem. Soc. Rev.* **2014**, *43*, 6116−6140.

(7) (a) Hu, Z.; Deibert, B. J.; Li, J. *Chem. Soc. Rev.* **2014**, *43*, 5815−5840. (b) Stavila, V.; Talin, A. A.; Allendorf, M. D. *Chem. Soc. Rev.* **2014**, *43*, 5994−6010. (c) Wang, C.; Zhang, T.; Lin, W. *Chem. Rev.* **2012**, *112*, 1084−1104. (d) Allendorf, M. D.; Bauer, C. A.; Bhaktaa, R. K.; Houka, R. J. T. *Chem. Soc. Rev.* **2009**, *38*, 1330−1352. (e) Bunzli, J. C. G.; Piguet, C. *Chem. Rev.* **2002**, *102*, 1897−1928.

(8) Kurmoo, M. *Chem. Soc. Rev.* **2009**, *38*, 1353−1379.

(9) (a) Zhu, Q.-L.; Xu, Q. *Chem. Soc. Rev.* **2014**, *43*, 5468−5512. (b) Falcaro, P.; Ricco, R.; Doherty, C. M.; Liang, K.; Hill, A. J.; Styles, M. J. *Chem. Soc. Rev.* **2014**, *43*, 5513−5560. (c) Furukawa, S.; Reboul, J.; Diring, S.; Sumida, K.; Kitagawa, S. *Chem. Soc. Rev.* **2014**, *43*, 5700−5734.

(10) (a) Liu, J.; Chen, L.; Cui, H.; Zhang, J.; Zhang, L.; Su, C.-Y. *Chem. Soc. Rev.* **2014**, *43*, 6011−6061. (b) Dhakshinamoorthy, A.; Garcia, H. *Chem. Soc. Rev.* **2014**, *43*, 5750−5765. (c) Corma, A.; Garcia, H.; Xamena, F. X. L. I. *Chem. Rev.* **2010**, *110*, 4606−4655. (d) Lee, J. Y.; Farha, O. K.; Roberts, J.; Scheidt, K. A.; Nguyen, S. B. T.; Hupp, J. T. *Chem. Soc. Rev.* **2009**, *38*, 1450−1459. (e) Ma, L.; Abney, C.; Lin, W. *Chem. Soc. Rev.* **2009**, *38*, 1248−1256.

(11) (a) Zhao, M.; Ou, S.; Wu, C.-D. *Acc. Chem. Res.* **2014**, *47*, 1199−1207. (b) Horike, S.; Dinca, M.; Tamaki, K.; Long, J. R. *J. Am. Chem. Soc.* **2008**, *130*, 5854−5855. (c) Roberts, J. M.; Fini, B. M.; Sarjeant, A. A.; Farha, O. K.; Hupp, J. T.; Scheidt, K. A. *J. Am. Chem. Soc.* **2012**, *134*, 3334−3337. (d) Wang, C.; Zheng, M.; Lin, W. *J. Phys. Chem. Lett.* **2011**, *2*, 1701−1709.

(12) Kumar, G.; Gupta, R. *Chem. Soc. Rev.* **2013**, *42*, 9403−9453.

(13) (a) Caron, S.; Dugger, R. W.; Ruggeri, S. G.; Ragan, J. A.; Ripin, D. H. B. *Chem. Rev.* **2006**, *106*, 2943−2989. (b) Sheldon, R. A.; Kochi, J. K. *Metal Catalyzed Oxidation of Organic Compounds*; Academic Press: New York, 1981. (c) Meunier, B. *Biomimetic Oxidations Catalyzed by Transition Metal Complexes*; Imperial College Press: London, 2000.

(14) (a) Fei, H.; Shin, J. W.; Meng, Y. S.; Adelhardt, M.; Sutter, J.; Meyer, K.; Cohen, S. M. *J. Am. Chem. Soc.* **2014**, *136*, 4965−4973. (b) Sen, R.; Saha, D.; Mal, M.; Brandao, P.; Rogez, G.; Lin, Z. *Eur. J. Inorg. Chem.* **2013**, 5020−5026. (c) Sen, R.; Saha, D.; Brandao, P.; Lin, Z. *Eur. J. Inorg. Chem.* **2013**, 5103−5109. (d) Rich, J.; Manrique, E.; Molton, F.; Duboc, C.; Collomb, M. N.; Rodriguez, M.; Romero, I. *Eur. J. Inorg. Chem.* **2014**, 2663−2670. (e) Zhang, J.; Biradar, A. V.; Pramanik, S.; Emge, T. J.; Asefa, T.; Li, J. *Chem. Commun.* **2012**, *48*, 6541−6543.

(15) (a) Xia, Q. H.; Ge, H. Q.; Ye, C. P.; Liu, Z. M.; Su, K. X. *Chem. Rev.* **2005**, *105*, 1603−1662. (b) Espinal, L.; Suib, S. L.; Rusling, J. F. *J. Am. Chem. Soc.* **2004**, *126*, 7676−7682.

(16) (a) Leadbeater, N. E.; Marco, M. *Chem. Rev.* **2002**, *102*, 3217−3274. (b) White, M. C.; Doyle, A. G.; Jacobsen, E. N. *J. Am. Chem. Soc.* **2001**, *123*, 7194−7195. (c) Shylesh, S.; Jia, M.; Thiel, W. R. *Eur. J. Inorg. Chem.* **2010**, 4395−4410.

(17) (a) Sheldon, R. A. *Metalloporphyrins in Catalytic Oxidations*; CRC Press: New York, 1994;. (b) Sharma, V. B.; Jain, S. L.; Sain, B. *Tetrahedron Lett.* **2003**, *44*, 383−386.

(18) Koya, S.; Nishioka, Y.; Mizoguchi, H.; Uchida, T.; Katsuki, T. *Angew. Chem., Int. Ed.* **2012**, *51*, 8243−8246.

(19) (a) Nam, W. *Acc. Chem. Res.* **2007**, *40*, 522−531. (b) Nam, W.; Lee, Y. M.; Fukuzumi, S. *Acc. Chem. Res.* **2014**, *47*, 1146−1154.

(20) (a) Wang, R.-M.; Hao, E.-X.; Shen, G.-R.; He, Y.-F.; Lei, Z.-Q. *J. Appl. Polym. Sci.* **2009**, *111*, 1999−2005. (b) Joseph, T.; Halligudi, S. B.; Satyanarayan, C.; Sawant, D. P.; Gopinathan, S. *J. Mol. Catal. A* **2001**, *168*, 87−97. (c) Lü, H.; Zhang, Y.; Jiang, Z.; Li, C. *Green Chem.* **2010**, *12*, 1954−1958. (d) Choudary, B. M.; Laxmikantam, M.; Rahman, A.; Reddy, C. V.; Rao, K. K. *Angew. Chem., Int. Ed.* **2001**, *40*, 763−766. (e) Woodham, A. P.; Meijer, G.; Fielicke, A. *Angew. Chem., Int. Ed.* **2012**, *51*, 4444−4447.

(21) Trost, B. M. *Science* **1991**, *254*, 1471−1477.

(22) (a) Roy, P.; Nandi, M.; Manassero, M.; Ricco, M.; Mazzani, M.; Bhaumik, A.; Banerjee, P. *Dalton Trans.* **2009**, 9543−9554. (b) Maksimchuk, N. V.; Timofeeva, M. N.; Melgunov, M. S.; Shmakov, A. N.; Chesalov, Y. A.; Dybtsev, D. N.; Fedin, V. P.;

Kholdeev, O. A. *J. Catal.* **2008**, *257*, 315−323. (c) Tonigold, M.; Lu, Y.; Bredenkötter, B.; Rieger, B.; Bahnmüller, S.; Hitzbleck, J.; Langstein, G.; Volkmer, D. *Angew. Chem., Int. Ed.* **2009**, *48*, 7546−7550. (d) Tonigold, M.; Lu, Y.; Mavrandonakis, A.; Puls, A.; Staudt, R.; Mçllmer, J.; Sauer, J.; Volkmer, D. *Chem.—Eur. J.* **2011**, *17*, 8671−8695. (e) Liu, Y. Y.; Leus, K.; Grzywa, M.; Weinberger, D.; Strubbe, K.; Vrielinck, H.; Deun, R. V.; Volkmer, D.; Speybroeck, V. V.; Voort, P. V. D. *Eur. J. Inorg. Chem.* **2012**, 2819−2827.

(23) (a) Ali, A.; Hundal, G.; Gupta, R. *Cryst. Growth Des.* **2012**, *12*, 1308−1319. (b) Kumar, G.; Aggarwal, H.; Gupta, R. *Cryst. Growth Des.* **2013**, *13*, 74−90. (c) Ali, A.; Bansal, D.; Gupta, R. *J. Chem. Sci.* **2014**, *126*, 1535−1546.

(24) (a) Mishra, A.; Ali, A.; Upreti, S.; Gupta, R. *Inorg. Chem.* **2008**, *47*, 154−161. (b) Mishra, A.; Ali, A.; Upreti, S.; Whittingham, M. S.; Gupta, R. *Inorg. Chem.* **2009**, *48*, 5234−5243. (c) Singh, A. P.; Gupta, R. *Eur. J. Inorg. Chem.* **2010**, 4546−4554. (d) Srivastava, S.; Ali, A.; Tyagi, A.; Gupta, R. *Eur. J. Inorg. Chem.* **2014**, 2113−2123.

(25) (a) Kumar, G.; Singh, A. P.; Gupta, R. *Eur. J. Inorg. Chem.* **2010**, 5103−5112. (b) Singh, A. P.; Ali, A.; Gupta, R. *Dalton Trans.* **2010**, *39*, 8135−8138. (c) Singh, A. P.; Kumar, G.; Gupta, R. *Dalton Trans.* **2011**, *40*, 12454−12461. (d) Kumar, G.; Gupta, R. *Inorg. Chem. Commun.* **2012**, *23*, 103−108. (e) Kumar, G.; Gupta, R. *Inorg. Chem.* **2012**, *51*, 5497−5499. (f) Kumar, G.; Gupta, R. *Inorg. Chem.* **2013**, *52*, 10773−10787. (g) Srivastava, S.; Dagur, M. S.; Gupta, R. *Eur. J. Inorg. Chem.* **2014**, 4966−4974.

(26) Perrin, D. D.; Armarego, W. L. F.; Perrin, D. R. *Purification of Laboratory Chemicals*; Pergamon Press: Oxford, 1980.

(27) *CrysAlisPro*, version 1.171.33.49b; Oxford Diffraction Ltd.: Abingdon, UK, 2009.

(28) Altomare, A.; Cascarano, G.; Giacovazzo, C.; Guagliardi, A. *J. Appl. Crystallogr.* **1993**, *26*, 343−350.

(29) Sheldrick, G. M. *Acta Crystallogr., Sect. A* **2008**, *64*, 112−122.

(30) Farrugia, L. J. *WinGX version 1.70, An Integrated System of Windows Programs for the Solution, Refinement and Analysis of Single-Crystal X-ray Diffraction Data*; Department of Chemistry, University of Glasgow: Glasgow, 2003.

(31) Spek, A. L.; PLATON, A. Multipurpose Crystallographic Tool, Utrecht University, The Netherlands, 2002.

(32) Nakamoto, K. *Infrared and Raman Spectra of Inorganic and Coordination Compounds*; Wiley: New York, 1997.

(33) Blatov, V. A.; Shevchenko, A. P.; Serezhkin, V. N. *J. Appl. Crystallogr.* **2000**, *33*, 1193−1193.

(34) Blatov, V. A.; O'Keefee, M.; Proserpio, D. M. *CrystEngComm* **2010**, *12*, 44−48.

(35) Network **3** is constituted of 1D chains connected through one of the Mn(II) ions; therefore, topological representation is not possible.

(36) (a) Kim, J.; Chen, B.; Reineke, T. M.; Li, H.; Eddaoudi, M.; Moler, D. B.; O'Keeffe, M.; Yaghi, O. M. *J. Am. Chem. Soc.* **2001**, *123*, 8239−8247. (b) Tranchemontagne, D. J.; Mendoza-Corté, J. L.; O'Keeffe, M.; Yaghi, O. M. *Chem. Soc. Rev.* **2009**, *38*, 1257−1283. (c) Shin, J. W.; Bae, J. M.; Kim, C.; Min, K. S. *Inorg. Chem.* **2013**, *52*, 2265−2267.

(37) Seth, P.; Bauzá, A.; Frontera, A.; Massera, C.; Gamez, P.; Ghosh, A. *CrystEngComm* **2013**, *15*, 3031−3039.

(38) Husain, A.; Ellwart, M.; Bourne, S. A.; Öhrström, L.; Oliver, C. L. *Cryst. Growth Des.* **2013**, *13*, 1526−1534.

(39) (a) Gong, Y.; Hao, Z.; Sun, J. L.; Shi, H.-F.; Jiang, P.-G.; Lin, J.-H. *Dalton Trans* **2013**, *42*, 13241−13250. (b) Nasani, R.; Saha, M.; Mobin, S. M.; Martins, L. M. D. R. S.; J. L. Pombeiro, A.; Kirillov, A. M.; Mukhopadhyay, S. *Dalton Trans* **2014**, *43*, 9944−9954.

(40) D'Vries, R. F.; Iglesias, M.; Snejko, N.; Gutiérrez-Puebla, E.; Monge, M. A. *Inorg. Chem.* **2012**, *51*, 11349−11355.

(41) Representative examples: (a) Yang, C.; Wang, X. P.; Omary, M. A. *J. Am. Chem. Soc.* **2007**, *129*, 15454−15455. (b) Kawano, M.; Kawamichi, T.; Haneda, T.; Kojima, T.; Fujita, M. *J. Am. Chem. Soc.* **2007**, *129*, 15418−15419. (c) Hwang, I. H.; Bae, J. M.; Kim, W. S.; Jo, Y. D.; Kim, C.; Kim, Y.; Kim, S. J.; Huh, S. *Dalton Trans.* **2012**, *41*, 12759−12765.

(42) (a) Choi, H. J.; Suh, M. P. *J. Am. Chem. Soc.* **2004**, *126*, 15844−15851. (b) Dang, D.; Wu, P.; He, C.; Xie, Z.; Duan, C. *J. Am. Chem. Soc.* **2010**, *132*, 14321−14323.

(43) (a) Lane, B. S.; Vogt, M.; DeRose, V. J.; Burgess, K. *J. Am. Chem. Soc.* **2002**, *124*, 11946−11954. (b) Godbole, M. D.; Hotze, A. C. G.; Hage, R.; Mills, A. M.; Kooijman, H.; Spek, A. L.; Bouwman, E. *Inorg. Chem.* **2005**, *44*, 9253−9266. (c) Zhong, S.; Fu, Z.; Tan, Y.; Xie, Q.; Xie, F.; Xhou, X.; Ye, Z.; Peng, G.; Yin, D. *Adv. Synth. Catal.* **2008**, *350*, 802−806. (d) Bruyneel, F.; Letondor, C.; Bastürk, B.; Gualandi, A.; Pordea, A.; Stoeckli-Evans, H.; Neier, R. *Adv. Synth. Catal.* **2012**, *354*, 428−440. (e) Rich, J.; Rodríguez, M.; Romero, I.; Fontrodona, X.; van Leeuwen, P. W. N. M.; Freixa, Z.; Sala, X.; Poater, A.; Solà, M. *Eur. J. Inorg. Chem.* **2013**, 1213−1224.

(44) The dimensions of a molecule were measured by selecting two suitable atoms followed by measuring their center-to-center distance in Chem3D (Chem3D Ultra 8.0; Cambridge Soft Corp.: Cambridge, MA, 2003) followed by addition of their van der Waals radii (Table S10, Supporting Information); see: (a) Gu, J.-M.; Kim, W.-S.; Huh, S. *Dalton Trans.* **2011**, *40*, 10826−10829. (b) Gu, J.-M.; Kwon, T.-H.; Park, J.-H.; Huh, S. *Dalton Trans.* **2010**, *39*, 5608−5610.

(45) Zeng, X.; Miao, C.; Wang, S.; Xia, C.; Sun, W. *RSC Adv.* **2013**, *3*, 9666−9669.

(46) Yonemitsu, M.; Tanaka, Y.; Iwamoto, M. *J. Catal.* **1998**, *178*, 207−213.

(47) Oldroyd, R. D.; Thomas, J. M.; Maschmeyer, T.; MacFaul, P. A.; Snelgrove, D. W.; Ingold, K. U.; Wayner, D. D. M. *Angew. Chem., Int. Ed. Engl.* **1996**, *35*, 2787−2790.

(48) Sebastian, J.; Jinka, K. M.; Jasra, R. V. *J. Catal.* **2006**, *244*, 208−218.

(49) The possibility of the allylic product to undergo propagation reaction is limited due to the nonavailability of the solvent, and no such products were obtained in our case.

(50) The *tert*-BuOH was observed in the gas chromatograph and quantified by comparison with a standard solution of known concentration.